Electrical and thermal conductivity of Al liquid at high pressures and temperatures from *ab initio* computations

Vojtěch Vlček,* Nico de Koker, and Gerd Steinle-Neumann
Bayerisches Geoinstitut, Universität Bayreuth, D-95440 Bayreuth, Germany
(Received 3 December 2011; revised manuscript received 29 February 2012; published 1 May 2012)

We performed first-principles calculations to obtain values of electrical (σ) and thermal conductivity (κ) for compressed aluminum liquid at temperatures and pressures up to 8000 K and 110 GPa. To do this we apply the Kubo-Greenwood formula via density functional perturbation theory to phase trajectories generated using first-principles molecular dynamics. Our results are consistent with measurements at low pressures, and indicate that electronic transport coefficients σ and κ increase under compression; with increasing temperature σ decreases and κ increases. Behavior in response to compression and heating are explained in terms of changes in occupation of conduction bands by thermally excited electrons. Based on the frequency dependence of σ, we further show that liquid aluminum is well described by the Drude picture over a wide range of conditions, confirming its free-electron nature. At high P and T, our computed σ and κ yield Lorenz numbers up to 7% lower than the theoretical value, indicating that the Wiedemann-Franz law remains approximately satisfied at extreme conditions. Using an electronically simple metal such as liquid Al as a guide to the behavior of more complex metals, we infer that present extrapolation-based estimates of σ and κ for the Earth's outer core may be 3–4 times too low.

DOI: 10.1103/PhysRevB.85.184201 PACS number(s): 72.15.Cz, 65.20.−w, 64.30.Ef

I. INTRODUCTION

The electronic transport properties of liquid metals at high pressures are crucial to understanding the processes associated with the formation and evolution of planetary cores. Differentiated terrestrial planets such as Earth contain metallic cores with iron as the primary element,[1,2] while interiors of the gas giants comprise cores which consist of hydrogen in the metallic state.[3,4] The electronic transport properties of liquid metals at extreme pressures and temperatures consequently control the generation of planetary magnetic fields by vigorous magnetohydrodynamic convection.[4,5]

Unfortunately, our current understanding of the high pressure behavior of σ and κ in liquid metals is based entirely on extrapolation of low pressure data and studies of solid metals.[6–9] No experimental data of electrical (σ) and thermal conductivity (κ) for metallic liquids at high pressures are available. Due to extreme technological challenges, experimental conductivity measurements are not yet feasible to perform. Current estimates of electronic transport properties in the Earth's core are based on extrapolations[10,11] of electrical conductivities obtained through shock-wave experiments,[7,12] which exhibit large uncertainties and describe the behavior solely along the Hugoniot in the phase stability region of solid Fe. Values of κ used in current thermal models for terrestrial planetary cores[13,14] are derived from extrapolations[10,11] of σ measurements via the Wiedemann-Franz law

$$\frac{\kappa}{\sigma} = LT, \tag{1}$$

where the Lorenz number L is theoretically expected to be $2.44 \times 10^{-8}\ \mathrm{W\,\Omega\,K^{-2}}$ (e.g., Ref. 15). The Wiedemann-Franz law is strictly valid for σ and κ that represent coefficients of linear response to applied time-invariant electrical field and thermal gradient.

First-principles calculations provide a direct and independent route to values of electrical and thermal conductivity, equally robust at ambient and extreme pressure conditions. Recent theoretical studies[16–23] of σ and κ employed the Kubo-Greenwood equations[24] within the framework of density functional theory (DFT),[25,26] closely reproducing the experimental data for liquids and plasmas of different metals.

In the current study, we apply this method to compressed liquid Al. Electronic transport properties of this material at low temperatures and/or low densities[17–19,22,27,28] have been widely studied using both theory as well as experiments, but the behavior of Al liquid under compression remains unexplored.

Al was chosen, since it is known to be well described by DFT (e.g., Refs. 29 and 30), and low pressure σ and κ obtained by the Kubo-Greenwood equation show good agreement with experiments.[17–19,22] Al is a simple metal with low number of valence electrons and free-electron-like behavior with low dispersion of electronic bands.[28] It is thus possible to compute the electronic transport properties with much less computational effort than, e.g., for Fe. Finally, we use our results to test the assumptions and scaling relations upon which existing estimates of σ and κ for the Earth's liquid outer core are based.

II. THEORETICAL BACKGROUND

Electrical and thermal conductivity represent a linear response of the system to applied electrical field and thermal gradient. If both of the external fields are applied simultaneously, the response is described by the Onsager kinetic coefficients matrix $\mathcal{L}_{ij}$ (Ref. 31),

$$\vec{j}_{\mathrm{el}} = \mathcal{L}_{11}\vec{E} + \mathcal{L}_{12}\vec{\nabla}T, \tag{2}$$

$$\vec{j}_{q} = \mathcal{L}_{21}\vec{E} + \mathcal{L}_{22}\vec{\nabla}T, \tag{3}$$

with electrical and thermal current densities $\vec{j}_{\mathrm{el}}$ and $\vec{j}_{q}$, respectively. The electronic transport properties then follow

 ©2012 American Physical Society

as

$$\sigma = \mathcal{L}_{11} \tag{4}$$

and

$$\kappa = \frac{1}{e^2 T}\left(\mathcal{L}_{22} - \frac{\mathcal{L}_{12}^2}{\mathcal{L}_{11}}\right), \tag{5}$$

with elementary charge e.

For external fields varying with frequency ω we can employ the Kubo formalism and write the Onsager kinetic coefficients as[22,32]

$$\mathcal{L}_{ij}(\omega) = (-1)^{i+j}\frac{\hbar e^2}{V_{\text{cell}}}\sum_{k',k}\mathcal{F}(\epsilon_k,\epsilon_{k'})\delta(\epsilon_k - \epsilon_{k'} - \hbar\omega) \times \langle\psi_k|\hat{\mathbf{v}}|\psi_{k'}\rangle\langle\psi_{k'}|\hat{\mathbf{v}}|\psi_k\rangle(\epsilon_k - \mu_e)^{i-1}(\epsilon_{k'} - \mu_e)^{j-1}, \tag{6}$$

with reduced Planck's constant $\hbar$, volume of the cell V_{cell}, ϵ_k the energy of eigenstate k, velocity operator $\hat{\mathbf{v}}$ acting on the wave function ψ_k, the electronic chemical potential μ_e, and $\mathcal{F}(\epsilon_k,\epsilon_{k'}) = f(\epsilon_k) - f(\epsilon_{k'})$ with the Fermi function f.

Through calculations using the *Abinit* software package[33] we access the Kohn-Sham wave functions, their energy eigenstates, and the electron velocities, calculated as the Brillouin zone gradient of the Hamiltonian $\partial\hat{H}/\partial\mathbf{k}$ using density functional perturbation theory. These quantities were subsequently employed for evaluation of Eq. (6) using the *Conducti* module.[22] The electronic density was computed using pseudopotentials with the generalized gradient approximation for exchange and correlation (PBE[34]). A 400 eV energy cutoff for the plane wave expansion was applied, and reciprocal space was sampled by a $2 \times 2 \times 2$ Monkhorst-Pack grid[35] of k points. We included in the calculations states at least to 6 eV above the Fermi energy. In this numerical implementation, the electronic eigenstates in Eq. (6) are convolved with a Gaussian of width $\Delta/\sqrt{2}$. The coefficients $\mathcal{L}_{ij}$ are evaluated at frequencies $\hbar\omega$ that correspond to integer multiples of Δ. Curves of $\sigma(\omega)$ and $\kappa(\omega)$ were found to be well characterized by $\Delta = 0.2$ eV. Lower values of the smearing factor result in strongly varying values of $\sigma(\omega)$ and $\kappa(\omega)$ due to limited number of energy eigenvalues ϵ_k; larger values of Δ do not fully capture the behavior of the electronic transport properties with frequency.

The computations of the electronic transport properties were performed for configurations obtained from phase trajectories generated using first-principles molecular dynamics simulations (FPMD) in the NVT ensemble. Cubic cells corresponding to five volumes between 0.6 and 1.0 V_{exp} were chosen, where $V_{\text{exp}} = 11.48$ cm^3 mol^{-1} is the volume of liquid Al at the ambient melting temperature.[36] Mean simulation temperatures were maintained via a Nosé thermostat,[37] with values of 2000, 3000, 4000, 6000, and 8000 K. Simulations span at least 20 ps, with a time step of 2 fs. For each system at P-T conditions above the theoretical melting curve[29] of Al, 10 uncorrelated atomic configurations were taken from the simulation trajectory to compute $\mathcal{L}_{ij}$.

For the FPMD simulations we employed the Vienna Ab-initio Simulation Package (VASP).[38] The electronic density at each simulation time step was calculated using the projector augmented wave formalism (PAW)[39] with the generalized gradient approximation for exchange and correlation (PBE)[34] using a 300 eV energy basis set cutoff. Reciprocal space sampling in the FPMD simulations was restricted to the Brillouin zone center.

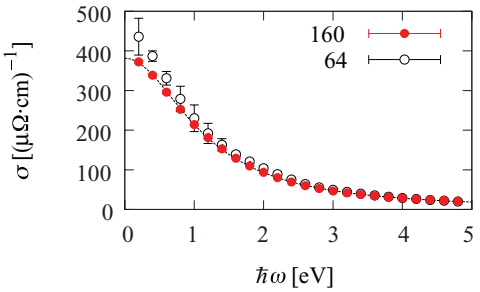

FIG. 1. (Color online) Frequency-dependent electrical conductivity $\sigma(\omega)$ obtained using a 160 atom supercell (filled circles) and a 64 atom supercell (open circles) for a volume of 0.6 V_{exp} at 4000 K. The dashed line represents a fit obtained through the Drude formula [Eq. (7)]. Each point represents a mean value over sampled configurations for the respective systems. Variations of the calculated values of σ (ω) among different configurations result in large standard deviations (represented by error bars) for cells containing 64 atoms; for 160 atoms simulation cells the error bars are smaller than the symbol size.

III. RESULTS

Zero-frequency values of $\sigma(\omega)$ and $\kappa(\omega)$ are obtained by extrapolation using the Drude formula[15]

$$\text{Re}[\sigma(\omega)] = \frac{\sigma_0}{1 + (\omega\tau)^2}. \tag{7}$$

with effective relaxation time τ, and σ_0 denoting the value in the dc limit. An analogous expression holds for the thermal conductivity.[15]

Monotonically decreasing curves with small uncertainties of $\sigma(\omega)$ are obtained for simulation cells containing 160 atoms (Fig. 1). Test simulations with 192 atoms at different volumes and temperatures indicate that σ_0 and κ_0 are converged to within the uncertainty quoted in Table I, reflecting the statistical sampling of the MD simulations. Similarly, using a denser k-point mesh ($4 \times 4 \times 4$) yields values for the transport properties within the quoted uncertainty.

The zero-frequency values of thermal and electrical conductivity obtained through Eq. (7) are listed in Table I, and the comparison with experimental data and previous calculations shown in Fig. 2. We see that values for σ_0 and κ_0 increase similarly under compression for all volumes investigated, but they show distinct temperature dependences: σ_0 decreases with temperature while κ_0 exhibits an opposite trend.

In the Drude picture, the response to an applied electrical field is assumed to be mediated by valence electrons exclusively, i.e., the number of valence electrons should be equal to the number of conduction electrons N_{eff} given as

$$N_{\text{eff}} = \frac{m\sigma_0}{e^2\tau}. \tag{8}$$

By using the fitted τ and σ_0 values from Eq. (7), we extract the effective number of conduction electrons for each V,T point.

TABLE I. Zero-frequency limits of the electrical and thermal conductivities for liquid Al calculated using 160 atom supercells. Numbers in brackets give the uncertainties in σ_0 and κ_0 due to the statistical sampling of 10 MD snapshots.

	1.0	0.9	0.8	0.7	0.6
V [V_{exp}]			$\sigma_0[(\mu\Omega\,\mathrm{cm})^{-1}]$		
2000 K	320 (10)	360 (11)	382 (9)	–	–
3000 K	280 (10)	322 (8)	350 (15)	370 (16)	–
4000 K	270 (11)	312 (8)	343 (7)	369 (9)	382 (4)
6000 K	240 (16)	273 (7)	311 (5)	341 (9)	361 (7)
8000 K	222 (7)	253 (9)	287 (7)	315 (8)	338 (5)
			$\kappa_0[\mathrm{W\,m^{-1}\,K^{-1}}]$		
2000 K	164 (5)	191 (5)	213 (4)	–	–
3000 K	200 (9)	236 (7)	260 (11)	280 (15)	–
4000 K	250 (10)	302 (8)	335 (8)	363 (9)	373 (4)
6000 K	350 (20)	398 (9)	449 (7)	486 (14)	507 (9)
8000 K	430 (10)	490 (17)	560 (13)	610 (15)	640 (10)

N_{eff} was found to be 2.8 ± 0.2 electrons for all conditions investigated.

Integrating $\sigma(\omega)$ in Eq. (7) over frequency leads to the sum rule

$$S = \frac{2mV_{\mathrm{atom}}}{\pi N e^2} \int_0^\infty \sigma(\omega) d\omega, \tag{9}$$

where N is the number of valence electrons and V_{atom} the cell volume per atom. For a fully free-electron metal, i.e., $N = 3$ in the case of Al, $S = 1$; as we find $N_{\mathrm{eff}} = 2.8 \pm 0.2$, S will be constrained to be smaller than the ratio of these two numbers (0.93). We find $S = 0.87 \pm 0.01$ for the simulations with 160 atom cells, and increasing the system size to 192 atoms does not change the result. This compares very favorably to results by Pozzo *et al.*[23] on liquid Na, where S is approximately 0.9 for even a larger number of atoms in the simulation cell.

IV. DISCUSSION

Our results indicate that the Drude picture provides a satisfactory description of electrical conductivity of liquid Al at conditions investigated. This is consistent with the work of Recoules *et al.*,[20] in which the $\sigma(\omega)$ curves provide N_{eff} slightly smaller than 3, and validates the assumption of Mostovych and Chan[28] for the extrapolation of conductivity data for Al plasma measured over a very limited frequency range to zero frequency.

The free-electron-like behavior is in contrast to the analysis of Knider *et al.*,[19] in which they claim that there is a significant contribution of electron transitions between eigenstates to electrical conductivity even at very low frequencies and that the Drude contribution is less than 0.1 of σ_0.

Despite the discrepancy in terms of the free-electron contribution between our computations and those of Knider *et al.*,[19] results for σ_0 are consistent between their and our work (Fig. 2), as well as with experimental data.[27] Comparison to experimental measurements of σ_0 and κ_0 in Al liquid are indirect,[27,40] as they are conducted at lower temperatures than those investigated in the current study.

Computations of Recoules and Crocombette[22] for a volume of 11.48 $\mathrm{cm^3\,mol^{-1}}$ at various temperatures agree reasonably with ours, with the small discrepancies likely stemming from their use of smaller supercells, which results in higher values of σ_0 and larger uncertainties (Fig. 1). A similar discrepancy is observed for their value of κ_0, again likely arising due to their smaller simulation cell. The values of Recoules and Crocombette[22] are thus not converged with respect to the number of atoms in the simulation cell.

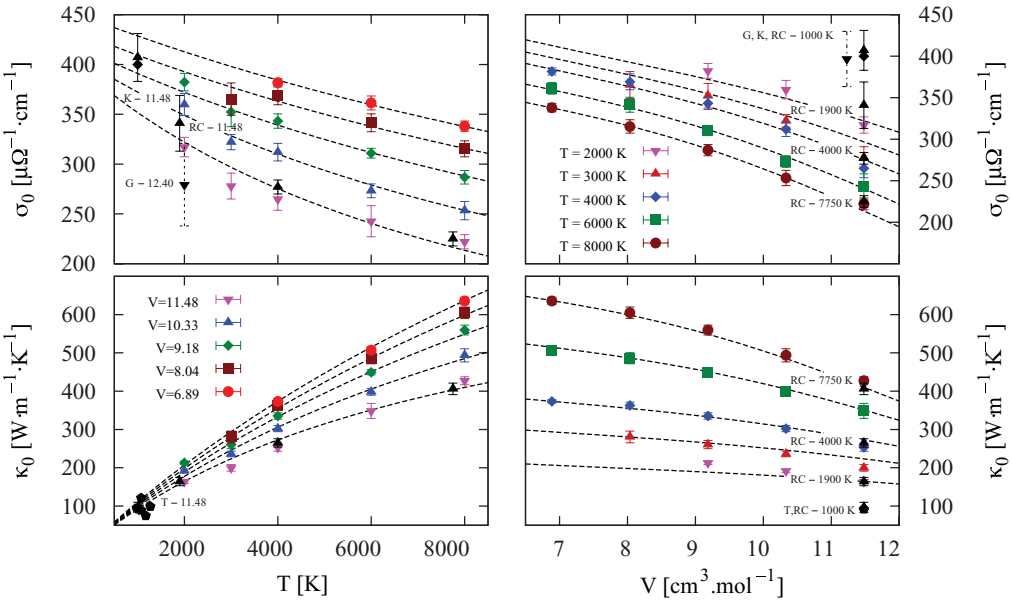

FIG. 2. (Color online) Results of this study at different temperatures and simulation cell volumes in units of $\mathrm{cm^3\,mol^{-1}}$ (indicated by different colors and symbols). Dashed lines denote the empirical model described in Appendix A. Experimental data of Gathers[27] (G, triangle down), Touloukian[40] (T, pentagon), and calculations by Recoules and Crocombette[22] (RC, triangle up), Knider *et al.*[19] (K, diamond), with temperatures and volumes (in units of $\mathrm{cm^3\,mol^{-1}}$) shown by black symbols for comparison.

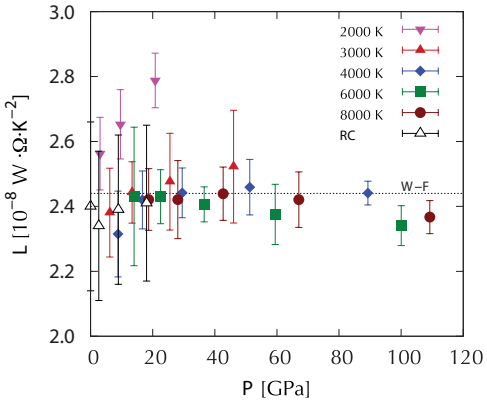

FIG. 3. (Color online) Calculated Lorenz number dependence on temperature and pressure is shown in comparison with the theoretical calculations by Recoules and Crocombette[22] (RC) at temperatures 1000, 1900, 4000, and 7750 K from lower to higher pressures.

In the zero-frequency limit we can translate the δ function in Eq. (6) into a simple derivative of the Fermi function with respect to electron scattering energy $\epsilon' = h\omega$. We can thus write $\sigma_0 \propto \partial f/\partial\epsilon'$. The decrease of σ_0 with T can therefore be attributed to temperature broadening of the Fermi function. Similar behavior is observed under decompression for both σ_0 and κ_0 due to charge localization and thus lower total $\partial f/\partial\epsilon'$. Conversely, the increase of thermal conductivity with T is governed by thermal excitation of electrons, i.e., the last two terms in Eq. (6) prevail over the temperature broadening of the Fermi function and lead to the increase of κ_0 with T.

Lorenz numbers determined from our first-principles results [Eq. (1)] illustrate that the Wiedemann-Franz law holds approximately at high temperatures, but is violated for temperatures below 3000 K (Fig. 3). Deviation from the Wiedemann-Franz law is attributed to nonelastic scattering of electrons, indicating that the electric and thermal currents are not affected by scattering in the same way.[15] The Wiedemann-Franz law generally holds at conditions at which electron scattering energy $|\epsilon_k - \epsilon_{k'}| \ll k_B T$, i.e., when the energy change due to scattering is effectively very small compared to the energy of the system. As the temperature decreases, this is no longer satisfied and we observe that L deviates from its theoretical value. We note that available data at ambient conditions for a diverse selection of metals show values ranging between 2.1 and 2.9 rather than a single number.[15] Our computed Lorenz numbers are therefore not unusual in their deviation from the theoretical value.

Using an empirical model for the V,T dependence of σ_0 and κ_0 (see Appendix A), together with a thermodynamic model for liquid Al constructed from our FPMD results (see Appendix B), we model the electronic transport properties along the theoretical melting curve of Al (Ref. 29). In Fig. 4 we show that electrical conductivity varies insignificantly, whereas thermal conductivity increases notably.

Since the electrical conductivity stays approximately constant, the Wiedemann-Franz law [Eq. (1)] dictates that the thermal conductivity is linearly proportional to temperature T. In other words, the change of thermal conductivity along the melting curve should be equal to the Clapeyron slope

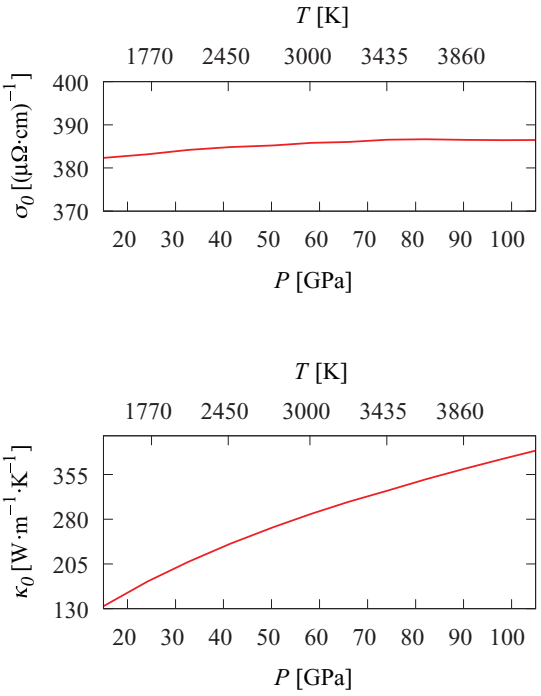

FIG. 4. (Color online) Electrical conductivity (top) and thermal conductivity (bottom) calculated for aluminum liquid for P,T conditions along the theoretical Al melting curve by Vočadlo and Alfè.[29]

of melting, i.e., $(\partial\kappa/\partial P)_{T_m} = dT_m/dP$. Therefore, in metals with strongly pressure dependent melting Clapeyron slopes, especially those showing maxima on the melting curves (e.g., Na, Pu—Ref. 41), the simple Lindemann-like scaling assumption that σ_0 is constant along the melting curve will most likely break down.

V. PLANETARY IMPLICATIONS

The current thermal models for terrestrial planetary cores[10,11,13,14] extrapolate the experimental values of electrical conductivity for Fe to the P,T conditions characteristic of planetary cores (for Earth's outer core: 3500–4500 K, 136 GPa at the core-mantle boundary and 5000–6000 K, 330 GPa at the inner core boundary[13,14,42,43]). This extrapolation was based on the following set of assumptions:[10,11] (a) electrical conductivity is inversely proportional to temperature, i.e., $\sigma_0 \propto 1/T$; (b) electrical conductivity is constant along the melting curve of the metal; (c) the Wiedemann-Franz law can be used for calculation of κ_0 from σ_0.

These assumptions remain untested in liquid metals at high P and T. Based on the premise that if an assumption fails for a simple metal liquid, it is unlikely to hold for a more complex transition metal or alloy, we investigate the validity of the above three assumptions for liquid Fe in the context of our results for Al.

In liquid Al the $1/T$ behavior is seen to be insufficient (Fig. 2), and would falsely predict a much steeper decrease of σ_0 with T. The relative decrease between 2000 and 4000 K is only about 12% for all the volumes investigated, whereas $1/T$ behavior requires a 50% decrease. If a similar T dependence holds for Fe, then the current estimates of the electrical

conductivity of the Earth's outer core may be too low by a factor of 3–4.

According to our results for aluminum liquid (Fig. 4) the value of the electrical conductivity along the melting curve can be considered constant to within 5% accuracy. We can therefore not disprove the validity of this assumption for pure Fe along its melting curve.

For liquid Al the high pressure Lorenz number is lower than the theoretical value by at most 7%. If the deviation is similar for Fe at pressures above 100 GPa, correct values of σ_0 would falsely lead to κ_0 values that are about 5%–10% too high. However, this is not sufficient to offset the discrepancy that would result from the strong underestimation of σ_0 due to its incorrectly assumed T dependence. Present estimates of κ_0 for Earth's core are therefore also likely to be 3–4 times too low. Moreover, the significant variation of κ_0 with P,T in Al liquid suggests that it will not be constant in planetary cores, as is generally assumed.[13,14]

VI. CONCLUSIONS

Our first-principles calculations for electrical and thermal conductivity of compressed liquid aluminum show strong dependence on pressure and temperature. The details of this dependence can be understood in terms of thermal excitation of electrons and increased occupation of conduction electronic states. We also demonstrate that liquid Al remains a free-electron-like metal at the conditions investigated. As a result, the extent to which the Wiedemann-Franz law is satisfied varies, with closest agreement to the theoretically expected scaling relation at high temperatures. Our results serve as a basic guide for the behavior of electronic transport properties in deep planetary cores, suggesting that current estimates for terrestrial planets may be quite far off.

ACKNOWLEDGMENTS

The authors appreciated discussions with Martin French, Stephan Kümmel, and Ronald Redmer. Anonymous reviews have significantly improved the manuscript. The work has been supported by the Deutsche Forschungsgemeinschaft (DFG) through Contract No. KO3958/2-1 in the focus program Planetary Magnetism. Computing facilities were provided in part by the Leibniz Supercomputer Centre of the Bavarian Academy of Sciences and Humanities.

APPENDIX A

For description of the V,T behavior of electrical and thermal conductivity we construct an empirical model for σ_0 based on the Bloch-Grüneisen formula,

$$\frac{1}{\sigma_0(V,T)} = a\left(\frac{V}{V_{\rm ref}}\right)^b + \left[c\left(\frac{V}{V_{\rm ref}}\right)^d + e\right]\left(\frac{T}{T_{\rm ref}}\right). \quad \text{(A1)}$$

TABLE II. Fit parameters of V,T-dependent model of electrical and thermal conductivity with reference volume $V_{\rm ref} = 11.48\ {\rm cm^3\ mol^{-1}}$ and temperature $T_{\rm ref} = 2000$ K.

a	$2.58 \times 10^3\ \Omega\,{\rm m}$
b	2.74×10^{-1}
c	$3.66 \times 10^2\ \Omega\,{\rm m}$
d	5.79
e	$1.60 \times 10^2\ \Omega\,{\rm m}$
f	$2.55 \times 10^{-8}\ {\rm W\,\Omega\,K^{-1}}$
g	3.66×10^{-2}
h	-4.46×10^{-2}

Thermal conductivity is described as

$$\kappa_0(V,T) = \left[f\left(\frac{V}{V_{\rm ref}}\right)^g\left(\frac{T}{T_{\rm ref}}\right)^h\right]\sigma_0(V,T)\,T. \quad \text{(A2)}$$

The fitting parameters are listed in Table II.

APPENDIX B

We provide a description of thermodynamic properties of the Al liquid over the whole range of conditions investigated, using the approach of de Koker and Stixrude,[44] with the temperature of onset for metallic behavior explicitly set to 0 K. The excess term was described by Eulerian finite strain and for the temperature dependence of the excess energy an exponent $m = 0.33$ was found to be optimal. In order to constrain the Helmoltz energy of liquid Al, the entropy was anchored by an experimental value[45] at 2000 K and 0 GPa, though it should be noted that this choice does not affect $E(V,T)$ and $P(V,T)$. The fit to the first-principles results and the fitting parameters are shown in Fig. 5 and Table III, respectively. The thermodynamic properties at 0 GPa and 2000 K are summarized in Table IV.

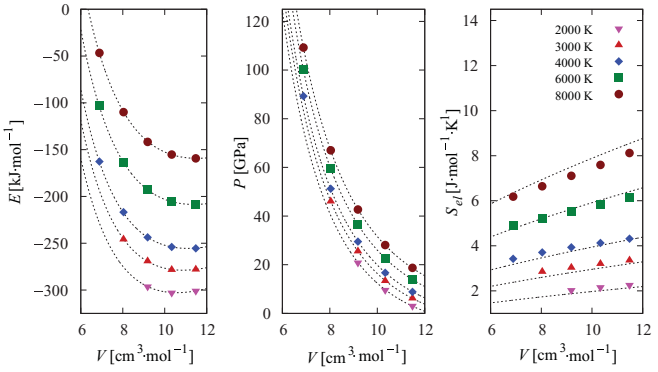

FIG. 5. (Color online) Equation of state fitted to the liquid Al FPMD simulation results for internal energy (left), pressure (middle), and electronic entropy (right). Error bars are smaller than the symbol size.

TABLE III. Fit parameters of the thermodynamic model for liquid Al equation of state at $P_0 = 0$ GPa and $T_0 = 2000$ K with reference volume $V_0 = 12.25$ cm^3 mol^{-1}. The total entropy at these conditions is fixed at its experimental value 95.7 J mol^{-1} K^{-1} (Ref. 45). For explanation of parameters, see de Koker and Stixrude.[44]

$F_{\rm xs}(V,T)$		
$F_{\rm xs0}$	-290	kJ mol^{-1}
$P_{\rm xs0}$	-1.46	GPa
$K_{T,\rm xs0}$	39	GPa
$K'_{T,\rm xs0}$	4	
$\alpha K_{T,\rm xs0}$	2.29×10^{-3}	GPa K^{-1}
$V_0\left(\frac{\partial \alpha K_T}{\partial V}\right)_{T,\rm xs0}$	-4.79×10^{-3}	GPa K^{-1}
$T_0\left(\frac{\partial \alpha K_T}{\partial T}\right)_{V,\rm xs0}$	-1.37×10^{-3}	GPa K^{-1}
$V_0^2\left(\frac{\partial^2 \alpha K_T}{\partial V^2}\right)_{T,\rm xs0}$	1.44×10^{-2}	GPa K^{-1}
$C_{V,\rm xs0}$	7.60	J mol^{-1} K^{-1}
$V_0\left(\frac{\partial C_V}{\partial V}\right)_{T,\rm xs0}$	11.2	kJ mol^{-1} K^{-1}
$V_0^2\left(\frac{\partial^2 C_V}{\partial V^2}\right)_{T,\rm xs0}$	4.18×10^{-2}	kJ mol^{-1} K^{-1}
$F_{\rm el}(V,T)$		
ζ_0	1.11	J mol^{-1} K^{-2}
ξ	0.58	

TABLE IV. Thermodynamic properties of the Al liquid at 0 GPa and 2000 K obtained from thermodynamic model fitted to FPMD results. Values at melting temperature and ambient pressure are shown for comparison where experimental data at $T = 2000$ K are not available.

	This study	Experiment	
V_0	12.25	12.40,[a] 13.17[†,b]	cm^3 mol^{-1}
K_T	40	28[g]–34[h]	GPa
K_S	51	50[*,c]	GPa
α	76	112,[*,d] 135[*,f]	$\times 10^{-6}$ K^{-1}
C_V	22.29	18.08[h]–21.30[g]	J mol^{-1} K^{-1}
C_P	28.00	31.75[e]	J mol^{-1} K^{-1}
γ	1.70	2.20[g]–2.80[h]	

[*]Value at melting temperature at $P = 0$ GPa; [†]extrapolated to $T = 2000$ K at $P = 0$ GPa; [a]Ref. 27; [b]Ref. 36; [c]Ref. 46; [d]Ref. 40; [e]Ref. 45; [f]calculated from Ref. 36; [g]calculated from Refs. 27, 46, 40, and 45; [h]calculated from Refs. 36, 46, and 45.

[*]vojtech.vlcek@uni-bayreuth.de

[1]F. Birch, J. Geophys. Res. **57**, 227 (1952).
[2]B. A. Buffet, Science **288**, 2007 (2000).
[3]E. Wigner and H. B. Huntington, J. Chem. Phys. **3**, 764 (1935).
[4]D. J. Stevenson, Earth Planet. Sci. Lett. **208**, 1 (2003).
[5]D. Gubbins, Phys. Earth Planet. Inter. **128**, 3 (2001).
[6]R. N. Keeler, *Physics of High Energy Density* (Academic Press, New York, 1971), Vol. 48.
[7]Y. Bi, H. Tan, and F. Jing, J. Phys.: Condens. Matter **14**, 10849 (2002).
[8]A. Balchan and H. Drickamer, Rev. Sci. Instrum. **32**, 308 (1961).
[9]R. Reichlin, Rev. Sci. Instrum. **54**, 1674 (1983).
[10]F. D. Stacey and O. L. Anderson, Phys. Earth Planet. Inter. **124**, 16382 (2001).
[11]F. D. Stacey and D. E. Loper, Phys. Earth Planet. Inter. **161**, 13 (2007).
[12]R. N. Keeler and A. C. Mitchel, Solid State Commun. **7**, 271 (1969).
[13]F. Nimmo, Treatise Geophys. **9**, 217 (2007).
[14]B. A. Buffet, Science **299**, 1675 (2003).
[15]N. W. Ashcroft and N. D. Mermin, *Solid State Physics* (Saunders College, Philadelphia, 1976).
[16]P. L. Silvestrelli, A. Alavi, and M. Parrinello, Phys. Rev. B **55**, 15515 (1997).
[17]P. L. Silvestrelli, Phys. Rev. B **60**, 16382 (1999).
[18]M. P. Desjarlais, J. D. Kress, and L. A. Collins, Phys. Rev. E **66**, 025401 (2002).
[19]F. Knider, J. Hugel, and A. V. Postnikov, J. Phys.: Condens. Matter **19**, 196105 (2007).
[20]V. Recoules, P. Renaudin, J. Clérouin, P. Noiret, and G. Zérah, Phys. Rev. E **66**, 056412 (2002).
[21]J. Clérouin, P. Renaudin, V. Recoules, P. Noiret, and M. P. Desjarlais, Contrib. Plasma Phys. **43**, 269 (2003).
[22]V. Recoules and J. P. Crocombette, Phys. Rev. B **72**, 104202 (2005).
[23]M. Pozzo, M. P. Desjarlais, and D. Alfè, Phys. Rev. B **84**, 054203 (2011).
[24]D. A. Greenwood, Proc. Phys. Soc. **71**, 585 (1958).
[25]P. Hohenberg and W. Kohn, Phys. Rev. **136**, B864 (1964).
[26]W. Kohn and L. J. Sham, Phys. Rev. **140**, A1133 (1965).
[27]G. R. Gathers, Int. J. Thermophys. **4**, 209 (1983).
[28]A. N. Mostovych and Y. Chan, Phys. Rev. Lett. **79**, 5094 (1997).
[29]L. Vočadlo and D. Alfè, Phys. Rev. B **65**, 214105 (2002).
[30]M. J. Tambe, N. Bonini, and N. Marzari, Phys. Rev. B **77**, 172102 (2008).
[31]L. Onsager, Phys. Rev. **37**, 405 (1931).
[32]B. Holst, M. French, and R. Redmer, Phys. Rev. B **83**, 235120 (2011).
[33]X. Gonze, Z. Kristallogr. **220**, 558 (2005).
[34]J. P. Perdew, K. Burke, and M. Ernzerhof, Phys. Rev. Lett. **77**, 3865 (1996).
[35]H. J. Monkhorst and J. D. Pack, Phys. Rev. B **13**, 5188 (1976).
[36]M. J. Assael, K. Kakosimos, R. M. Banish, J. Brillo, I. Egry, R. Brooks, P. N. Quested, K. C. Mills, A. Nagashima, Y. Sato *et al.*, J. Phys. Chem. Ref. Data **35**, 285 (2006).
[37]S. Nose, J. Chem. Phys. **81**, 511 (1984).
[38]G. Kresse and J. Furthmüller, Phys. Rev. B **54**, 11169 (1996).

[39]G. Kresse and D. Joubert, Phys. Rev. B **59**, 1758 (1999).
[40]Y. S. Touloukian, *Thermal Conductivity, Metallic Elements and Alloys, Thermophysical Properties of Matter Vol. 1: Thermal conductivity of metallic elements and alloys* (IFI/Plenum, New York, 1970).
[41]D. A. Young, *Phase Diagrams of the Elements* (University of California Press, Berkeley, CA, 1991).
[42]A. M. Dziewonski and D. L. Anderson, Phys. Earth Planet. Inter. **25**, 297 (1981).
[43]D. Alfè, G. D. Price, and M. J. Gillan, J. Phys. Chem. Solids **65**, 1573 (2004).
[44]N. de Koker and L. Stixrude, Geophys. J. Int. **178**, 162 (2009).
[45]H. P. D. R. Stull, *JANAF Thermochemical Tables*, 2nd ed. (Dow Chemical Company, Thermal Research Laboratory, Washington, DC, 1971).
[46]L. F. Mondolfo, *Aluminum Alloys: Structure and Properties* (Butterworths, London, 1976).